JGR Biogeosciences

RESEARCH ARTICLE
10.1029/2025JG009584

Putative Analogs of Pyrite Suns Forming in Proglacial Alaska Mudflats

Heather L. Fair[1], Trinity L. Hamilton[1,2], and Jeff R. Havig[1,3]

[1]Department of Plant and Microbial Biology, University of Minnesota, Saint Paul, MN, USA, [2]The Biotechnology Institute, University of Minnesota, Saint Paul, MN, USA, [3]Department of Earth Sciences, University of Minnesota, Minneapolis, MN, USA

Key Points:

- Disc-shaped pyrite suns of Pennsylvanian age are interpreted as an abiotic oddity forming deep within shale
- We compared the morphology of pyrite suns with proglacial mud precursors of Alaska and examined the microbial communities of the mud
- We present initial data supporting our observed hypothesis that pyrite suns may be forming at the earth surface in proglacial Alaska

Supporting Information:

Supporting Information may be found in the online version of this article.

Correspondence to:

T. L. Hamilton,
trinityh@umn.edu

Citation:

Fair, H. L., Hamilton, T. L., & Havig, J. R. (2026). Putative analogs of pyrite suns forming in proglacial Alaska mudflats. *Journal of Geophysical Research: Biogeosciences*, *131*, e2025JG009584. https://doi.org/10.1029/2025JG009584

Received 25 NOV 2025
Accepted 23 APR 2026

Author Contributions:

Conceptualization: Heather L. Fair, Trinity L. Hamilton
Data curation: Heather L. Fair
Formal analysis: Heather L. Fair
Funding acquisition: Heather L. Fair, Trinity L. Hamilton
Investigation: Heather L. Fair
Methodology: Heather L. Fair, Trinity L. Hamilton
Project administration: Heather L. Fair
Resources: Heather L. Fair, Trinity L. Hamilton
Software: Heather L. Fair
Supervision: Trinity L. Hamilton, Jeff R. Havig
Validation: Heather L. Fair, Trinity L. Hamilton, Jeff R. Havig
Visualization: Heather L. Fair
Writing – original draft: Heather L. Fair

Abstract Disc-shaped pyrite suns of the Pennsylvanian age Anna Shale are thought to have formed where pressure restricted pyrite crystal growth to a flattened disc shape during diagenesis at the Anna Shale and the underlying Herrin coal boundary. Others have proposed syndepositional involvement of sulfate-reducing bacteria in the depositional environment. We hypothesize that the first steps in pyrite sun formation occur in mudflats of proglacial Alaska, with cyanobacterial mats trapping glacier silts within extracellular polymeric substances where microbial communities interact with allochthonous hydrocarbons, sulfur, and iron to precipitate amorphous iron sulfide minerals. We compared pyrite sun morphology with pyrite sun precursor formations, used 16S rRNA amplicon sequencing to investigate putative pyrite-forming bacteria, and determined iron content and mineralogy using XRD and sequential iron extraction of Matanuska Glacier mudflats sampled in June 2023. Recovered 16S rRNA sequences include EPS-generating cyanobacteria (*Aphanizomenon NIES81*), sulfur cycling bacteria (e.g., *Thiobacillus*, *Sulfuritalea*, *Desulfovibrio*), and iron cycling bacteria (e.g., *Rhodoferax*, *Geobacter*). In our proposed model, methane and hydrogen sulfide generated within anoxic mud form gas domes in benthic silt resting in a disc shape at the air-water interface. Iron sulfides precipitate below the surface of the cyanobacterial mats and are later buried and transformed into pyrite crystals with diagenesis across the disc shape. This combination of high organic carbon availability with sulfur and iron cycling and resulting iron sulfide mineral precipitation across a sharp redox gradient in depositional silt is a close match to the ancient depositional environment of the pyrite sun containing unit within the Anna Shale.

Plain Language Summary Pyrite suns have been interpreted as an abiotic oddity generated during diagenetic processes after deposition. Here we examine mechanisms that may form pyrite suns in proglacial mudflats of an Alaskan glacier where pools of anoxic glacier silts provide the substrate for hypothesized cyanobacteria mat-driven microbially induced sedimentary structures. Examining this process will increase our knowledge of how microbial and abiotic processes within extreme environments may form the precursors to pyrite suns. Disentangling the abiotic and biotic mechanisms of pyrite formation can help us to understand ancient landscapes, serve as proxies for life on other planets, and help us better understand the probable origins of life on earth.

1. Introduction

Pyrite suns are rare in the rock record and occur at the interface of Herrin (No. 6) coal and overlying Anna Shale layers of the Sparta coal region in Illinois (Dyson, 2019) where coal miners pulled them from shale ceilings to sell to collectors (Figure 1a). To date, there is no validated explanation of how the 300-million-year-old disc-like structures ranging in size from a thumbprint to a large disc-shaped crystallization of pyrite (FeS_2) originated (Elrick, 2018). The prevailing explanation is that pyrite suns form deep within shale (Seilacher, 2001) with the involvement of sulfate-reducing bacteria (SRB), which are promoters of >90% of pyrite formed in sediment environments (Rickard, 2015). A depositional environment similar to the Illinois swamps along the ancient inland sea during the Paleozoic Era has also been proposed (Elrick, 2018, Dyson, 2019). However, the genesis of pyrite suns has thus far eluded a definitive explanation—with geologists maintaining a curiosity about the latitudinal line visible in lithified pyrite suns thought to be a nucleation site for pyrite crystals (Figure 1b) (Žorž, 2022).

Glacier mudflats along the lakeshores of the Matanuska Glacier moraine are underlain by subglacial ice (Figure 1c) containing high concentrations of sulfate (SO_4^{2-}) and nitrate (NO^{3-}) (Kiyani et al., 2018). Hydrocarbons emanate into the mudflats from marine sandstone and shale sequences of the underlying Matanuska

Writing – review & editing: Heather L. Fair, Trinity L. Hamilton, Jeff R. Havig

formation, which contains subbituminous and anthracite coal (Payne & Hopkins, 1945; Speight, 2020; Trop & Plawman, 2006). The Matanuska Glacier is also underlain to the east by the Lower Jurassic Talkeetna Volcanic Formation, the most well-preserved oceanic volcanic arc in the world (Clift et al., 2005). Gabbros containing up to 15% magnetite from the middle crust penetrate basaltic, andesitic, and dacitic volcanic flows, which are underlain by the lower ultramafic rocks along the Border Ranges fault system (Burns, 1983; Clift et al., 2005). The northward dipping Talkeetna Arc contains several E-W strike-slip faults, including through the Matanuska River Valley (Smart et al., 1996).

Based on field observations, we hypothesize that cyanobacteria mat microbial communities and abiotic processes form precursors of pyrite suns in proglacial mudflats in Alaska. We suggest that in anoxic mud below biofilms, sulfide production from the activity of SRB along with microbially mediated iron redox transformations and methanogenesis work in concert with water level, hydrocarbon dynamics, and the Marangoni effect (mass transfer along a fluid surface caused by a gradient in surface tension) to produce pyrite sun precursors containing organic matter in the form of hydrocarbons and microbial cell byproducts. With burial, subsurface conditions are anoxic and reduced iron monosulfides precipitate within porewater interstitial spaces. Greater crystal overgrowth, cementation, and diagenesis of FeS across the disk-shaped precursor into pyrite are hypothesized to occur at shallow depths.

To examine our hypothesis, we compared the morphology of ∼300 Mya lithified pyrite suns with glacier silt pyrite precursors, which may fall into the category of microbially induced sedimentary structures (Bose & Chavetz, 2009; Noffke, 2009, 2010). We also compared the environmental conditions of the Herrin coal to Anna Shale depositional transition with the Matanuska terminal moraine lakeshore mudflats, conducted 16S rRNA sequencing to characterize the microbial composition of glacier silt pyrite precursors from the Matanuska Glacier terminal moraine in 2023, and determined iron content and associated mineralogy using XRD and sequential iron extraction on precursor mudflat silts.

2. Materials and Methods

2.1. Morphological and Environmental Comparison

To examine our hypothesis, we measured the diameter of the pyrite sun precursor formations in proglacial mudflats and compared these to the diameter of pyrite suns in images from the Anna Shale. We also took digital images of the precursors showing how they cluster within the most stagnant mudflats and how the fine morphological features of pyrite sun precursors form in the silt above the waterline. We also compared the environmental conditions of the Herrin coal to Anna Shale depositional transition with the Matanuska terminal moraine lakeshore mudflats.

2.2. Microbial Community Collection and Characterization

Using aseptic techniques, we collected microbial subsamples from 12 precursor formations at the Matanuska Glacier terminal moraine area in June 2023 and froze the samples until further processing in the lab. We extracted DNA from the precursor mud samples by using DNA Miniprep Isolation Kits (Zymo Research, Tustin, CA, USA) and bulk DNA concentrations were determined using a Qubit dsDNA HS Assay kit (Molecular Probes, Eugene, OR, USA) and Qubit Fluorometer (Invitrogen, Carlsbad, CA, USA). We submitted DNA to the University of Minnesota Genomics Center for amplicon sequencing targeting the V4 region of the 16S rRNA gene. Dual indexed Nextera XT DNA libraries were prepared with an improved protocol enabling detection of taxonomic groups that are often undetected (Gohl et al., 2016) and sequenced using a 2 × 300 v3 flow cell (Illumina, San Diego, CA, USA). The DADA2 workflow was conducted on demultiplexed samples with primers removed to obtain identified amplicon sequencing variants (ASVs) representing our response variables (Callahan et al., 2016). Paired-end raw reads were processed to denoise, detect, and remove chimeras, and taxonomy assigned to ASVs at known taxonomic levels using the SILVA database (v138, 29). Before conducting statistical analyses, singletons, unidentified ASVs at the genera and class level, mitochondrial DNA, and chloroplast sequences were removed from the data set.

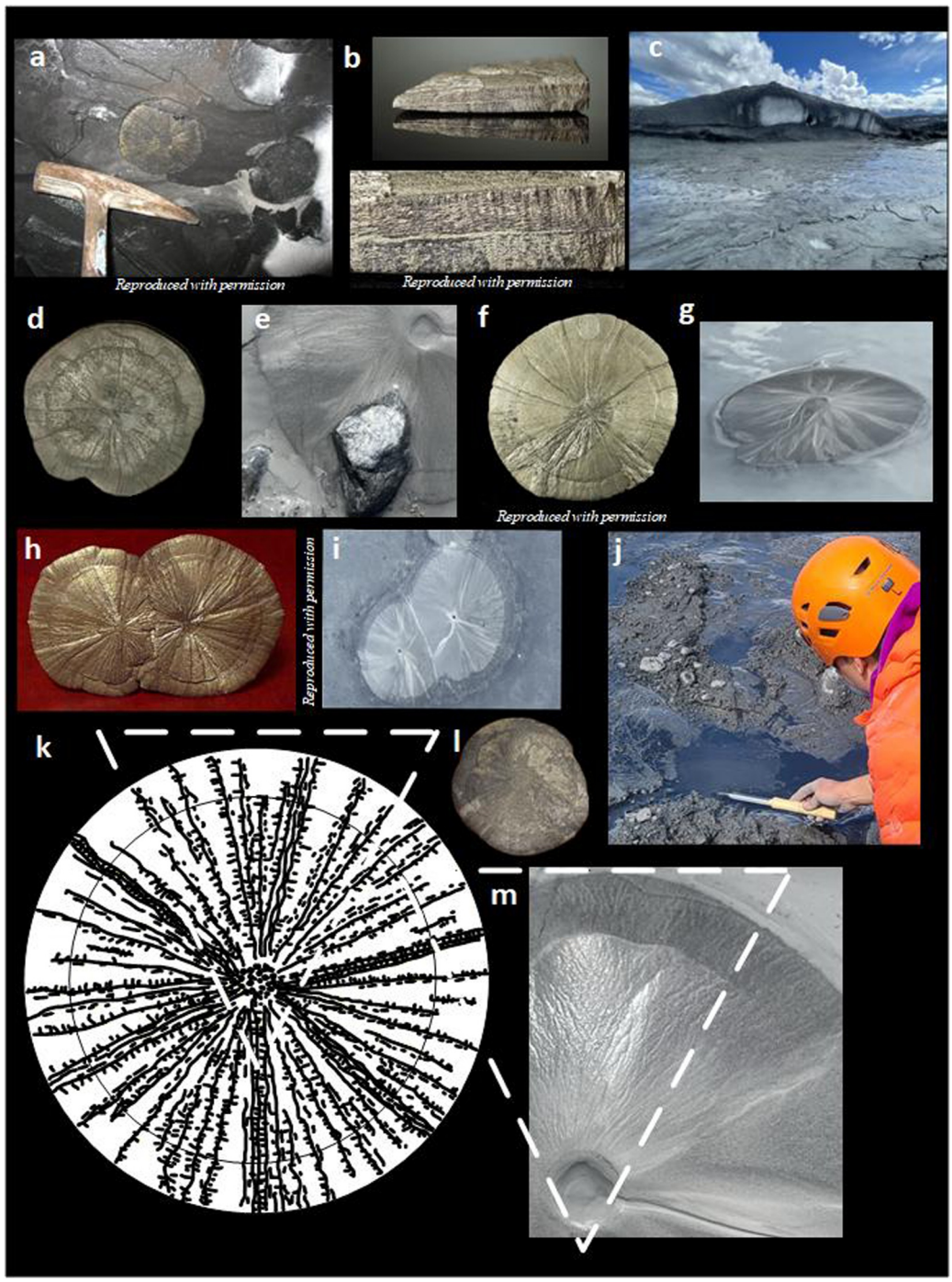

Figure 1. Geological setting where pyrite suns and precursors are found and morphological comparison of lithified pyrite suns and pyrite sun precursors. Pyrite suns are found in the shale ceilings of coal mines in Sparta, Illinois (a). The blackened latitudinal line within pyrite suns is the possible nucleating site for pyrite crystals (b, top) and the internal herringbone pattern of pyrite and shale are visible within the magnified image of the same pyrite sun (b, bottom). Mudflats composed of saturated glacial silts at the proglacial lakeshore at the Matanuska Glacier Alaska where precursors were forming (c). Morphological comparison of pyrite sun with notch in outer perimeter and pyrite sun precursor growing around gravel, which is forming a notch (d and e). Secondary layer of pyrite emanating from the central depression in lithified pyrite sun (f) and similar formation with silts emanating from the central water filled depression in pyrite precursor (g). Coalesced pyrite suns are found in the rock record (h) and within the glacier mudflats (i). Sampling sediments from a pool with hydrocarbons (j). Circumference lines at approximately 80 percentile of pyrite sun circumference (d, f, h, l) can be seen forming in pyrite precursors from changing water lines and hydrocarbons (e, i, m). The central depression in lithified pyrite suns (d, f, h, l) and water-filled depression in the middle of pyrite precursors (e, g, i, m). Superficial features of fine lines and cracks can be seen radiating from the central hole in both the ancient pyrite suns and the pyrite precursor (d, f, h, k, l, m). Diameters of pyrite suns and precursors are within the image credits.

2.3. XRD and Sequential Iron Extraction

We collected additional mud from two precursor formations for X-ray diffraction (XRD) analysis and from five precursor and mudflat samples to conduct sequential iron extraction (Claff et al., 2010; Sohlenius & Öborn, 2004). The sequential iron extraction method allowed for the partitioning of organic and pyrite-bound iron to be distinguished using a one-step method for acid sulfate soils (Claff et al., 2010). Dried sediment samples were mounted on standard recessed slide mounts (20 × 20 × 0.5 mm) for XRD. The data were collected on a Rigaku MiniFlex 600 with Cu Ka radiation and a Ni filter. The samples were scanned from 15° to 80° at 1 deg./min. Phase ID analysis was performed using MDI Jade (version 9.5; Materials Data: Livermore, CA, 2019) and the Crystallography Open Database (COD) (Gražulis et al., 2012). Quantification was performed using Jade's Whole Pattern Fitting and standard reference intensity ratio (RIR) factors.

3. Results

3.1. Morphological and Environmental Comparison

The morphological similarities between the pyrite sun precursors and Paleozoic pyrite suns include similar size and congruent coarse and fine morphological features (Figures 1d–1m). Pyrite suns can have notches similar to a pyrite precursor forming around moraine gravel (Figures 1d and 1e). Secondary layers of pyrite appear to emerge and lithify from a central depression in pyrite suns and in pyrite sun precursors, sediments are emitted from a depression in the center of the pyrite precursors to form a pattern similar to that of lithified pyrite suns (Figures 1f and 1g). The pattern of coalesced pyrite discs from the rock record were seen in coalesced sedimentary pyrite sun precursors (Figures 1h and 1i). Žorž (2022) described internal herringbone patterns in pyrite suns with dark bands of shale and pyrite. Pyritized bacteria similar to pyritized Trilobites in shale (Briggs et al., 1991) could be forming in the glacial mud with hydrocarbons, which is visible in the interior of a pyrite sun (Figure 1b). Lithified pyrite suns have a depression in the center (Figures 1d, 1f, 1h, and 1k), which is consistent with our observations of central water filled depressions of pyrite precursors (Figures 1e, 1g, 1i, and 1m) (Žorž, 2022).

Figure 1 *Image credits*: Image a (S. Elrick), Image b top and bottom (I. Dolinar, 4.5 cm), Image c (H. Fair), Image d (H. Fair, Disc diameter: 7.6 cm), Image e (H. Fair, Precursor diameter: 9 cm), Image f (arkenstone/www.irocks.com, Disc diameter: 10 cm), Image g (H. Fair, Precursor diameter: 19 cm), Image h (T. Kennedy, right disc diameter: 10 cm), Image i. (H. Fair, right precursor diameter: 23 cm), Drawing k (H. Fair), Image l (H. Fair, Disc diameter: 9 cm), Image m (H. Fair, Precursor diameter: 9 cm).

3.2. Microbial Community Characterization

In the subsamples of precursor formations from the mudflats, microbial genera involved in biochemical reactions that can form pyrite included sulfur oxidizers, sulfate reducers, iron cycling microbes, hydrocarbon producers and scavengers, methanotrophs, and denitrifiers (Table 1). Our samples taken from the top surface of the mud had average relative abundances of sulfur oxidizing bacteria (e.g., *Thiobacillus*, *Sulfuritalea*, and *Sulfurifustis*) ranging from 4% to 23% of the known ASVs and average relative abundance of the iron cycling bacteria *Rhodoferax* ranging from 10% to 20% of the known ASV genera. The relative abundance of methanotrophs ranged from 3% to 5%. In addition, we include the results from supraglacial cryoconite hole microbial communities to show the stark contrast of microbial community structure compared with the mudflat results, especially with the key microbial genera involved in pyrite formation which are either not present or in low proportions of the total ASVs in the cryoconite holes (Table 1).

3.3. XRD and Sequential Iron Results

Mature pyrite crystals were not detected in the two pyrite precursors by XRD (Figures S1 and S2 in Supporting Information S1). The silt sampled from the two precursor samples contained crystals of Quartz (SiO_2) (29% and 27%), Albite ($Na(AlSi_3O_8)$) (27% and 43%), Clinochlore ($Mg5Al(AlSi_3O_{10})(OH)_8$) (18% and 5%) and Muscovite $KAl_2(AlSi_3O_{10})(OH)_2$ (17% in the first sample). Other crystals detected at <5% were Carbon (C_8), Pumpellyite ($Ca_2XAl_2[Si_2O_6(OH)][SiO_4](OH)_2A$), Ammonium Hydrogen Phosphate ($(NH_4)(?)$ (H_2PO_4) (H_3PO_4), Scawtite ($(Ca_7(Si_3O_9)2CO_3 \cdot 2H_2O$) and Clinozoisite ($((Ca_2Al_3)[SiO_4][Si_2O_7]$ O(OH)) (Figures S1 and S2 in Supporting Information S1). Non-pyrite sulfide minerals (7.5%–10.7%) were likely extracted during the HCL step of the

Table 1
Mean Proportion of Microbial Genera Putatively Involved in Pyrite Formation Biochemical Reactions Within Mudflats at the Glacier Forefront

Microbial groups	HCP	MF1	MF2	CH
Sulfur Oxidizers				
Thiobacillus	0.030	0.053	0.200	<0.001
Sulfuritalea	0.001	0.001	0.013	0.000
Sulfurifustis	0.003	0.006	0.012	0.000
Sulfuricurvum	0.001	0.003	0.004	0.000
Sulfurisoma	0.000	0.007	0.004	0.000
Sulfuricella	0.000	0.000	0.002	0.000
Total	0.035	0.071	0.233	<0.001
Sulfate Reducers				
Desulfovibrio	0.001	0.012	0.005	0.000
Desulfocapsa	0.000	0.002	0.000	0.000
Bilophila	0.000	0.002	0.000	0.000
Desulfuromonas	0.000	<0.001	<0.001	0.000
Total	0.001	0.020	0.009	0.000
Iron Reducers/Oxidizers				
Rhodoferax	0.200	0.165	0.100	0.005
Geobacter	0.000	<0.001	<0.001	0.000
Gallionella	0.000	0.001	<0.001	0.000
Total	0.200	0.170	0.100	0.005
Hydrocarbon Producers/Scavangers				
Aphanizomenon NIES81	0.131	0.001	0.040	0.000
Pseudanabaena PCC-7429	0.020	0.000	0.002	0.016
Novosphingobium	0.005	0.001	0.010	0.023
Pseudomonas	0.002	0.019	0.011	0.000
Anabaena PCC-7122	0.000	0.000	0.002	0.000
Total	0.159	0.021	0.060	0.039
Methanotrophs				
Methylotenera	0.043	0.017	0.023	0.002
Pseudomonas	0.002	0.019	0.011	0.000
Methylobacterium-Methylorubrum	0.002	0.009	0.001	0.000
Methylibium	0.002	0.000	0.002	0.000
Methylobacter	0.000	0.000	0.001	0.000
Total	0.050	0.045	0.037	0.002
Denitrifiers				
Thiobacillus	0.030	0.053	0.198	0.000
Pseudomonas	0.002	0.019	0.011	0.000
Allorhizobium-Neorhizobium-Pararhizobium-	0.002	0.024	0.010	0.000
Bradyrhizobium	0.001	0.003	0.000	0.006
Mesorhizobium	0.000	0.000	0.000	0.000
Total	0.034	0.098	0.219	0.006

Note. Glacier surface cryoconite holes (CH) are included for comparison. Hydrocarbon pool (HCP) in mudflat 1 (Figure 1j), Mudflat 1 (MF1) with stagnant water and mature pyrite sun precursors, Mudflat 2 (MF2) with slight flow and pyrite sun precursors and cryoconite holes (CH). Cryoconite holes are meltwater-filled depressions with cryoconite substrate (i.e., cyanobacteria and microbial communities that form around sediment) on the clean ice surface of the Matanuska Glacier, Glacier View, AK, 2023.

sequential iron extraction, but these could also be Fe-containing carbonates, ferrihydrite, hematite, or jarosite. Pyrite was detected in sequential iron extractions from the samples ranging from 5% to 7% and 76%–83% of the sample contents were likely comprised of magnetite, goethite, and/or Fe-containing primary silicate minerals (Table S1 in Supporting Information S1).

4. Discussion

4.1. Pyrite Sun Formation Process

The glacier terminal moraine, where pyrite sun precursors are forming, represents a dynamic environment where geophysical controls impact microbial processes. Glacial grinding of bedrock generates abundant fine-grained, reactive mineral surfaces including iron-bearing phases, while meltwater redistribution from proglacial lakes to lakeshores creates quiescent, mudflat zones with intermittent shallow pools within glacier flour at the ice and proglacial lake margins. In some glacier moraine settings, hydrocarbons or reduced fluids migrating from depth can further supply electron donors for biogeochemical processes to occur. Together, these factors create chemically stratified, anoxic microenvironments favorable for microbial sulfate reduction and iron sulfide precipitation.

DNA sequencing comparing glacier surface cryoconite hole sediments and glacier forefront mudflat sediments demonstrates how distinct geophysical conditions of sediment supply, meltwater hydrology, redox gradients, and organic inputs may structure microbial community composition and metabolic potential (Table 1). Glacier dynamics may act to regulate the geochemical conditions that determine which microbial processes dominate, including those involved in sulfide mineral formation.

Moreover, the initial morphological examination of pyrite suns and pyrite sun precursors showed shared macroscopic and fine morphological structural characteristics, which supports the hypothesis that pyrite sun formation begins at the earth's surface before burial, compaction, and diagenesis. The most developed precursor formations were in small, closed basins (i.e., pools or mudflats) along the proglacial lakeshores, which had the most stagnant conditions. Hydrocarbons were present in the water column and floating on the surface where they adhered to the precursor formations, which gradually accumulated silts and became exposed above the water line. The predominant clay/silt substrate in the pools with pyrite sun precursors contrasted with nearby moraine pools. The moraine pools with no precursor formations had gravel and cobble substrates and visible cyanobacteria blooms, highlighting the importance of black shale-forming conditions for the formation of pyrite sun precursors. The depositional environment at the Matanuska Glacier with allochthonous carbons, iron, and sulfur are similar to the Paleozoic Era depositional wetlands that formed shale along the ancient inland sea of Sparta, IL, which we suggest were similar to our modern observations in Alaska.

Here we suggest the overarching physical and biological process for the formation of pyrite sun precursors and potential diagenesis into pyrite in shale-forming proglacial mudflats with steep gradient oxic/anoxic conditions (Figure 2). Mudflats in proglacial Alaska contain shallow pools (0–5 cm) with glacier silt substrate. Beneath the benthic silt, gases generated by methanogens and SRB lift the silt into domes (Voorhies et al., 2012) (Figure 2a) that carry hydrocarbons into the water column from a central hole and gradually reach the air-water interface (Figures 2a and 2b). Sheath-forming microbes generate mats that capture silt in EPS, which maintain microbes and silt in the recognizable pyrite sun precursor template and provide nucleation sites for iron monosulfides (Figures 1e, 1g, 1i, and 1m). As the biofilm spreads, Marangoni-effect patterns form by the interaction of water, hydrocarbons, and silt (Figure 2c) which may later become the lithified lines radiating from the center depression (Figures 1d, 1f, 1h, and 1l). Glacial sedimentation processes cover and bury pyrite sun precursor formations, creating subsurface anoxic conditions which set the stage for further porewater precipitation of reduced iron monosulfides. These conditions would then allow for greater crystal overgrowth, cementation, and diagenesis of FeS across the disk-shaped precursor into pyrite within the shale-forming environment at shallow depths (Figure 2d).

In the black shale clay and depositional environment of the proglacial lakeshore, rapid burial and pyrite formation follow well-established diagenetic controls and microbial activity with early oxygen consumption, reducing pore waters, shallow sulfate reduction resulting in high sulfide concentrations at the surface, preservation of organic matter, and reactive iron leading to early amorphous iron monosulfides. With rapid burial, pyrite may cement

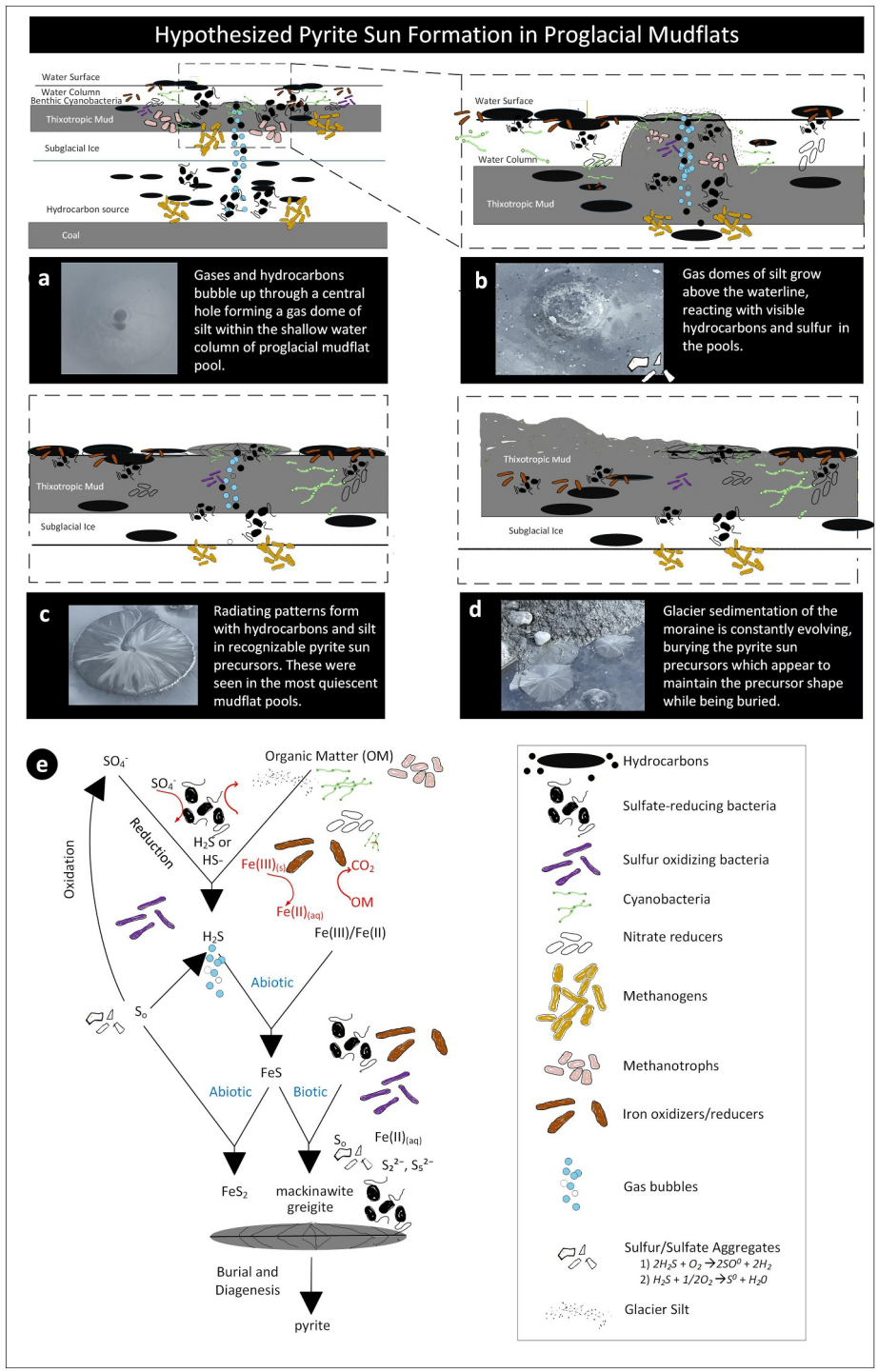

Figure 2. Visual process describing the formation of pyrite sun precursors in a proglacial mudflat pool (a–d) and biogeochemical reactions occurring (e). The Matanuska Valley is underlain by coal and sandstones, which release hydrocarbons that move to the surface and emerge in glacier mudflats. Within mudflat pools, gas domes of clay silt form in the water, emitting gases and transporting hydrocarbons through a nascent pyrite precursor silt mound (a). As the silt dome grows, it comes into contact with floating hydrocarbons and sulfur at the water surface (b). Silts spread out into a pyrite precursor shape with recognizable patterns seen in lithified pyrite suns (c). Pyrite precursors become buried in glacier mud (d). Diagenesis into pyrite suns is hypothesized to continue with burial. The biotic and abiotic processes of sulfate reduction, and carbon, iron, and sulfur cycling through the polysulfide pathway are depicted in the pyrite sun formation diagram (e). Legend is within the box at bottom right.

sediments and protect the microtextures found in the precursor formation, which later develops crystal overgrowths with burial. We suggest that this process could also occur in similar, stagnant, shale-forming mudflats of quick-clay that were the precursor to the Anna Shale where preserved pyrite suns are found.

4.2. Microbial Community Characterization

The relative abundance of 16S rRNA microbial sequences supports our hypothesis that precursors of pyrite (e.g., amorphous FeS, mackinawite (FeS_{mack}), and greigite (Fe_3S_4)) are forming under thin cyanobacteria mats on the glacier mudflat surface. Cyanobacteria mats are stratified with multiple layers of microbes and can have a steep oxic-anoxic gradient. We hypothesize that diazotrophic *Aphanizomenon* NIES81 (0.15%–14%) arranges in sheaths and controls buoyancy, which may diurnally position pyrite sun precursors above the surface of the water to avoid hydrocarbons when accessing sunlight (Cirés & Ballot, 2016) (Table 1). We suggest that within the cyanobacterial mats, the polysulfidic FeS_2 pathway occurs, transforming sulfur (S^0) into a pool of intermediate sulfur species through dissimilatory oxidation, reduction, and disproportionation (Rickard, 2015; Sekerci et al., 2025).

Sulfur oxidizing bacteria are important producers of sulfate, which SRB reduces to sulfide (Figure 2e, Table 1). 16S rRNA sequences of sulfate reducing bacteria (e.g., *Desulfovibrio*, *Desulfocapsa*, and *Bilophila*) indicate sulfate reduction to sulfide in the anoxic biofilm layer, which could contribute to FeS and pyrite formation. Sequences affiliated with dissimilatory iron-reducing *Rhodoferax* (1.0%–44.3%) were recovered, which could transform ferric iron (Fe^{3+}) to ferrous iron (Fe^{2+}), with the Fe^{2+} reacting with byproducts of SRB metabolism (H_2S/HS^-) to form metastable iron monosulfide (FeS) (Rickard, 2015). This may be the dark latitudinal line seen in pyrite suns serving as the nucleation site for pyrite (Figure 1b) (Feng et al., 2014; Hodges, 1992).

4.3. XRD and Sequential Iron Extraction

The results of the sequential iron extractions substantiate the presence of metastable iron, which can later form pyrite intermediaries and supports our polysulfide pathway of pyrite formation (Table S1 in Supporting Information S1). Aqueous FeS at circumneutral pH can nucleate into less soluble FeS minerals such as mackinawite (FeS_{mack}) or greigite (Fe_3S_4) which can both form pyrite (FeS_2) (Boyd & Payne, 2025; Kappler et al., 2021; Rickard, 2015; Thiel et al., 2019; Wächtershäuser, 1988, 1990). The conversion to pyrite (FeS_2) can occur within days (Donald & Southam, 1999) or it might take years or centuries in the earth's subsurface. With the supporting geological evidence of the Talkeetna Volcanic Arc and Tonsina ultra-mafic assemblage underlying the Matanuska Glacier, which have the potential to supply iron and sulfur, and the release of hydrocarbons from shale, sandstones, and underlying coal, we propose that the pyrite sun formations are likely forming in this environment. Paige and Knopf (1907) provide additional evidence for the potential of pyrite diagenesis in shale by describing rare balls and scales of pyrite found within the bituminous coal in the eastern district of the lower Matanuska Valley, which could be similar to pyrite suns.

5. Conclusion

In this initial pilot study, we provide preliminary evidence for our hypothesis that the formation of pyrite suns is microbially induced within mudflats of Alaskan glaciers. Future research directions for constraining the mechanisms of the polysulfide pathway and diagenesis of precursors into pyrite suns are needed, but this initial examination shows that processes which occurred 280–300 million years ago giving rise to precursor stages of pyrite suns in a swampy depositional environment may be occurring in modern glacial environments of Alaska.

Conflict of Interest

The authors declare no conflicts of interest relevant to this study.

Availability Statement

The sequencing data for this study have been deposited in the NCBI BioProject database (Fair et al., 2026a). The data analysis file is available online at figshare (Fair et al., 2026b), copyright CC BY 4.0. No code was created as part of this research.

Acknowledgments
This work was funded by the National Science Foundation (Grants 2010852 and 2113784). We thank E. Beer for fieldwork assistance, P.C. Smiley, Jr. for review of the early manuscript, B. Stevenson for field access, S. Elrick, J. Dyson, M. Žorž, I. Dolinar, E. Hood and J. Fellman, University of Alaska Southeast, C. Hanson, S. Whitacre, the University of Minnesota Supercomputing Institute, and A. Michaud, Byrd Polar and Climate Research Center, The Ohio State University for supporting roles in this research.

References

Bose, S., & Chavetz, H. S. (2009). Topographic control on distribution of modern microbially induced sedimentary structures (MISS): A case study from Texas coast. *Sedimentary Geology*, *213*, 136–149. https://doi.org/10.1016/j.sedgeo.2008.10.009

Boyd, E. S., & Payne, D. (2025). Expanded diversity of microbial groups capable of anaerobic pyrite reduction and assimilation of dissolution products. *Environmental Microbiology*, *27*(6), e70125. https://doi.org/10.1111/1462-2920.70125

Briggs, D. E. G., Bottrell, S. H., & Raiswell, R. (1991). Pyritization of soft-bodied fossils: Beecher's trilobite bed, Upper Ordovician, New York State. *Geology*, *19*(12), 1221–1224. https://doi.org/10.1130/0091-7613(1991)019<1221:POSBFB>2.3.CO;2

Burns, L. E. (1983). The Border Ranges ultramafic and mafic complex, south-central Alaska: Cumulate fractionates of island-arc volcanics. *Canadian Journal of Earth Sciences*, *22*(7), 1020–1038. https://doi.org/10.1139/e85-106

Callahan, B. J., McMurdie, P. J., Rosen, M. J., Han, A. W., Johnson, A. J. A., & Holmes, S. P. (2016). DADA2: High-resolution sample inference from Illumina amplicon data. *Nature Methods*, *13*(7), 581–583. https://doi.org/10.1038/nmeth.3869

Cirés, S., & Ballot, A. (2016). A review of the phylogeny, ecology and toxin production of bloom-forming *Aphanizomenon* spp. and related species within the Nostocales (cyanobacteria). *Harmful Algae*, *54*, 21–43. https://doi.org/10.1016/j.hal.2015.09.007

Claff, S. R., Sullivan, L. A., Burton, E. D., & Bush, R. T. (2010). A sequential extraction procedure for acid sulfate soils: Partitioning of iron. *Geoderma*, *155*(3–4), 224–230. https://doi.org/10.1016/j.geoderma.2009.12.002

Clift, P. D., Draut, A. E., Kelemen, P. B., Blusztajn, J., & Greene, A. (2005). Stratigraphic and geochemical evolution of an oceanic arc upper crustal section: The Jurassic Talkeetna Volcanic Formation, south-central Alaska. *GSA Bulletin*, *117*(7), 902–925. https://doi.org/10.1130/B25638.1

Donald, R., & Southam, G. (1999). Low temperature anaerobic bacterial diagenesis of ferrous monosulfide to pyrite. *Geochimica et Cosmochimica Acta*, *63*(13–14), 2019–2023. https://doi.org/10.1016/S0016-7037(99)00140-4

Dyson, J. R. (2019). Geochemistry and organic petrography of the Anna shale (Pennsylvanian) and the occurrence of pyrite "suns" in Southwestern Illinois (Master's thesis). OpenSIUC. Retrieved from https://opensiuc.lib.siu.edu/theses/2579

Elrick, S. (2018). *Pyrite suns: Unique mineral treasures of Illinois*. Illinois State Geological Survey, Prairie Research Institute. Retrieved from https://www.ideals.illinois.edu/items/110037

Fair, H., Hamilton, T. L., & Havig, J. R. (2026a). Alaska pyrite sun precursor formations in proglacial mudflats [Dataset]. *National Center for Biotechnology Information BioProject PRJNA1445464*. https://www.ncbi.nlm.nih.gov/bioproject/PRJNA1445464

Fair, H., Hamilton, T. L., & Havig, J. R. (2026b). Pyrite Sun precursor 16S amplicon sequencing data [Dataset]. *figshare*. https://doi.org/10.6084/m9.figshare.31926525.v3

Feng, Z. Y., Fan, C. X., Huang, W. Y., & Ding, S. M. (2014). Microorganisms and typical organic matter responsible for lacustrine "black bloom". *Science of the Total Environment*, *470–471*, 1–8. https://doi.org/10.1016/j.scitotenv.2013.09.022

Gohl, D. M., Vangay, P., Garbe, J., MacLean, A., Hauge, A., Becker, A. B., et al. (2016). Systematic improvement of amplicon marker gene methods for increased accuracy in microbiome studies. *Nature Biotechnology*, *34*(9), 942–949. https://doi.org/10.1038/nbt.3601

Gražulis, S., Daškevič, A., Merkys, A., Chateigner, D., Lutterotti, L., Quirós, M., et al. (2012). Crystallography open database (COD): An open-access collection of crystal structures and platform for world-wide collaboration. *Nucleic Acids Research*, *40*(D1), 420–427. https://doi.org/10.1093/nar/gkr900

Hodges, C. F. (1992). Interaction of cyanobacteria and sulfate-reducing bacteria in subsurface black-layer formation in high-sand content golf greens. *Soil Biology and Biochemistry*, *24*, 15–20. https://doi.org/10.1007/BF00010178

Kappler, A., Bryce, C., Mansor, M., Lueder, U., Byrne, J. M., & Swanner, E. D. (2021). An evolving view on biogeochemical cycling of iron. *Nature Reviews Microbiology*, *19*(6), 360–374. https://doi.org/10.1038/s41579-020-00502-7

Kiyani, M. R., Doyle, S. M., Sangwan, N., Wang, G. Q., Gilbert, J. A., Christner, B. C., & Zhu, T. F. (2018). Metagenomic analysis of basal ice from an Alaskan glacier. *Microbiome*, *6*, 123–127. https://doi.org/10.1186/s40168-018-0505-5

Noffke, N. (2009). The criteria for the biogenicity of microbially induced sedimentary structures (MISS) in Archean and younger, sandy deposits. *Earth-Science Reviews*, *96*(3), 173–180. https://doi.org/10.1016/j.earscirev.2008.08.002

Noffke, N. (2010). *Geobiology: Microbial mats in sandy deposits from the Archean era to today*. Springer-Verlag. https://doi.org/10.1007/978-3-642-12772-4

Paige, S., & Knopf, A. (1907). Reconnaissance in the Matanuska and Talkeetna basins, with notes on the placers of the adjacent region. In *U.S. Geological Survey, Report of progress of investigations of mineral resources of Alaska in 1906* (Vol. 314, pp. 104–125). U.S. Geological Survey Bulletin. https://doi.org/10.3133/b327

Payne, T. G., & Hopkins, D. M. (1945). Geology and coal resources of the western part of the lower Matanuska Valley coal field, Alaska. *US Geological Survey Open-File Report*, *28*, 45–100. https://doi.org/10.3133/ofr45100

Rickard, D. (2015). *Pyrite: A natural history of fool's gold*. Oxford University Press. https://doi.org/10.1093/oso/9780190203672.003.0006

Seilacher, A. (2001). Concretion morphologies reflecting diagenetic and epigenetic pathways. *Sedimentary Geology*, *143*(1–2), 41–57. https://doi.org/10.1016/S0037-0738(01)00092-6

Sekerci, F., Fischer, S., Joshi, P., Peiffer, S., Kappler, A., & Mansor, M. (2025). Sulfur microenvironments as hotspots for biogenic pyrite formation. *Scientific Reports*, *15*(1), 20148. https://doi.org/10.1038/s41598-025-05178-8

Smart, K. J., Pavlis, T. L., Sisson, V. B., Roeske, S. M., & Snee, L. W. (1996). The Border Ranges fault system in Glacier Bay National Park, Alaska: Evidence for major late Mesozoic–early Cenozoic dextral strike-slip motion. *Canadian Journal of Earth Sciences*, *33*(9), 1268–1282. https://doi.org/10.1139/e96-096

Sohlenius, G., & Öborn, I. (2004). Geochemistry and partitioning of trace metals in acid sulphate soils in Sweden and Finland before and after sulphide oxidation. *Geoderma*, *122*(2–4), 167–175. https://doi.org/10.1016/j.geoderma.2004.01.006

Speight, J. (2020). Origin and properties of oil shale. In *Chapter in shale oil and gas production processes* (pp. 671–714). Gulf Professional Publishing. https://doi.org/10.1016/C2015-0-06314-6

Thiel, J., Byrne, J. M., Kappler, A., Schink, B., & Pester, M. (2019). Pyrite formation from FeS and H2S is mediated through microbial redox activity. *Proceedings of the National Academy of Sciences USA*, *116*(14), 6897–6902. https://doi.org/10.1073/pnas.1814412116

Trop, J. M., & Plawman, T. L. (2006). *Bedrock geology of the Glenn Highway from Anchorage to Sheep Mountain, Alaska—Mesozoic-Cenozoic forearc basin development along an accretionary convergent margin: Field guide*. Alaska Geological Survey.

Voorhies, A. A., Biddanda, B. A., Kendall, T., Jain, S., Marcus, D. N., Nold, S. C., et al. (2012). Cyanobacterial life at low O_2: Community genomics and function reveal metabolic versatility and extremely low diversity in a Great Lakes sinkhole mat. *Geobiology*, *10*(3), 250–267. https://doi.org/10.1111/j.1472-4669.2012.00322.x

Wächtershäuser, G. (1990). Evolution of the first metabolic cycles. *Proceedings of the National Academy of Sciences USA*, *87*(1), 200–204. https://doi.org/10.1073/pnas.87.1.200

Wächtershäuser, G. (1988). Pyrite formation, the first energy source for life: A hypothesis. *Systematic and Applied Microbiology*, *10*(3), 207–210. https://doi.org/10.1016/S0723-2020(88)80001-8

Žorž, M. (2022). Pyrite Suns from Randolph County, Illinois. *Rocks & Minerals*, *97*, 330–347. https://doi.org/10.1080/00357529.2022.2053628